Transition in swimming direction in a model self-propelled inertial swimmer

Thomas Dombrowski, Shannon K. Jones, Georgios Katsikis, Amneet Pal Singh Bhalla, Boyce E. Griffith, and Daphne Klotsa

Phys. Rev. Fluids **4**, 021101 — Published 8 February 2019

DOI: 10.1103/PhysRevFluids.4.021101

Transition in swimming direction in a model self-propelled inertial swimmer

Thomas Dombrowski,[1,*] Shannon K. Jones,[2,*] Georgios Katsikis,[3]
Amneet Pal Singh Bhalla,[4,5] Boyce E. Griffith,[6] and Daphne Klotsa[2,†]

[1]*Department of Physics, The University of North Carolina at Chapel Hill, Chapel Hill, NC, USA*
[2]*Department of Applied Physical Sciences, The University of North Carolina at Chapel Hill, Chapel Hill, NC, USA*
[3]*Koch Institute for Integrative Cancer Research, Massachusetts Institute of Technology, Cambridge, Massachusetts, USA*
[4]*Applied Numerical Algorithms Group, Lawrence Berkeley National Laboratory, Berkeley, CA, USA*
[5]*Mechanical Engineering, San Diego State University, CA, USA*
[6]*Departments of Mathematics, Applied Physical Sciences, and Biomedical Engineering, The University of North Carolina at Chapel Hill, Chapel Hill, NC, USA*

(Dated: December 20, 2018)

We propose a reciprocal, self-propelled model swimmer at intermediate Reynolds numbers (Re). Our swimmer consists of two unequal spheres that oscillate in antiphase generating nonlinear steady streaming (SS) flows. We show computationally that the SS flows enable the swimmer to propel itself, and also switch direction as Re increases. We quantify the transition in the swimming direction by collapsing our data on a critical Re and show that the transition in swimming directions corresponds to the reversal of the SS flows. Based on our findings, we propose that SS can be an important physical mechanism for motility at intermediate Re.

PACS numbers: May be entered using the `\pacs{#1}` command.

Understanding motility requires connections between fundamental physics and biology [1–3] and has many applications, including drug-delivering nanomachines [4, 5] and autonomous underwater vehicles [6–8]. Swimming regimes can be classified by the Reynolds number (Re), which characterizes the relative importance of inertial over viscous forces. Although there is a large body of work on motility in Stokes flows ($Re \ll 1$), in which viscous forces dominate, and at high Re ($Re \gg 1$), in which inertial forces dominate, less is known about the intermediate regime $Re_{\text{int}} \sim 1 - 1000$ [2, 9, 10].

The Re_{int} regime encompasses an enormous diversity of organisms, ranging from larvae (of *e.g.* fish, squid, ascidian) and large ciliates, to nematodes, copepods, plankton and jellyfish, that exhibit a variety of motility mechanisms: jet propulsion [11, 12], anguilliform locomotion [13–17], rowing [18, 19], aquatic flapping flight [20], and ciliate beating [21, 22]. Plankton have even been proposed to contribute to the large-scale transport of nutrients and dissolved gases in the ocean [23–27]. However, most prior studies on Re_{int} motility have focused on the details of specific organisms [11–14, 16–22, 24, 25, 28]. As a result, few general models exist for motility at Re_{int}; examples are an extension of the Stokesian squirmer to include inertia [27, 29–33], which makes assumptions about the generation of flow due to small-amplitude oscillations on the surface of a spherical swimmer and the flapping-plate model, which is a lumped-torsional-flexibility model that uses passive pitching and responds to an actuation [34, 35]. However, there is a lack of understanding regarding the unifying physical mechanisms that swimmers at Re_{int} exhibit. To achieve this, more models with varying degrees of freedom that operate under different conditions at Re_{int} are needed. Only then can we make progress in better understanding biological swimmers and designing artificial ones at intermediate scales.

Steady streaming (SS) is the nonzero, time-averaged flow that arises at Re_{int} due to oscillations of a rigid body in a fluid and has been studied for various cases, such as around a single sphere [36–40], cylinder, near a wall. While SS has been used to manipulate particles *e.g.* [41–45] and cells [46] via *external* vibrations, it has not been used as a mechanism for self-propulsion, even though there have been suggestions that it may be relevant for the enhanced motility of *Synechococcus* cyanobacteria [47].

In this letter we propose a simple, reciprocal, and self-propelled model swimmer, termed the *spherobot*, that uses steady streaming flows in a novel way, *i.e.* for propulsion. The spherobot is composed of two unequal spheres that oscillate with respect to each other, in antiphase, generating SS flows, Fig. 1(a). We computationally studied the spherobot's motility over a broad range of parameters: viscosity, sphere amplitudes, distance between the spheres, sphere radii and sphere-radii ratio. At $Re = 0$, the spherobot cannot swim because of Purcell's scallop theorem [48]; its reciprocal stroke does not break time-reversal symmetry. At low, nonzero Re the spherobot started to swim and, interestingly, switched swimming direction from a small-sphere-leading to a large-sphere-leading regime. We found that the point of transition collapsed to a critical value when the appropriate Reynolds number was used, which revealed a strong dependence on the SS flows of the small sphere. Analyzing the flow fields, we showed that the transition in swimming direction corresponds to the reversal of SS flows around the spherobot that occurs as the Reynolds num-

* Contributed equally
† dklotsa@email.unc.edu

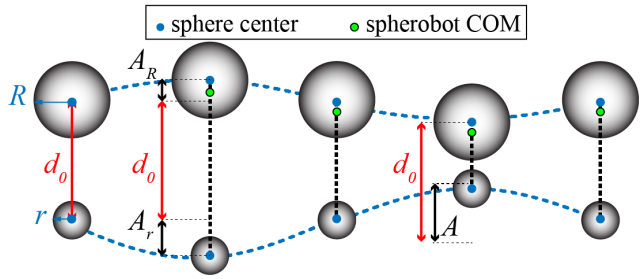

FIG. 1. Reciprocal oscillation of the spherobot swimmer over one cycle. Spheres' centers of mass (COM)(blue circles) and the spherobot COM (green circle) are indicated. The distance between the spheres' centers, $d(t)$, is d_0, at the equilibrium distance, $d_0 - A$, minimum distance and $d_0 + A$ at maximum distance. The total amplitude $A = A_R + A_r$.

ber increases.

Methods. The spherobot was composed of two unequal spheres with radii r, R, which were coupled to one another by prescribing the distance between their centers. To model this computationally, we tethered the two spheres using an active spring with a time-dependent distance $d(t) = d_0 + A\sin(\omega t)$, in which d_0 is the equilibrium distance between the sphere centers, $A = 0.5(d_{\max} - d_{\min})$ is the amplitude of the spherobot, and ω is the frequency of oscillation (Fig. 1). Equal and opposite (spring) forces were applied to the spheres that acted to keep them approximately at the prescribed distance apart (error $\approx 10^{-7}$m). Thus, the model ensures a geometrically reciprocal cycle and a force-free swimmer. Because the same force is applied to both spheres, the one with the smaller mass (the small sphere) will have a larger amplitude A_r than the one with the bigger mass (large sphere), A_R, (*i.e.* if $r \leq R$ then $A_r \geq A_R$). In most simulations we have $A_r \approx 4A_R$. The amplitude of the spherobot A is the sum of the two, $A = A_r + A_R$, Fig.1. Both spheres were neutrally buoyant with respect to the surrounding fluid. To simulate the spherobot in a fluid, we used an exactly constrained immersed boundary (CIB) method [49, 50]. The CIB scheme is implemented in IBAMR [51, 52], which provides several variants of the immersed boundary (IB) method [53] for fluid-structure interaction. The spherobot was immersed in a fluid that occupied a finite cell with no-slip walls. The visualization and analysis of the flow fields was done in VisIt [54]. Further details on the model and method are given in the Supplemental Material (SM) [55].

The swimming velocity of the spherobot was measured after steady state had been reached and was defined as the net displacement of the spherobot center of mass over one cycle. We defined the Reynolds number as $Re = A_r r/\delta^2 = A_r r\omega/\nu$ because, as we will show, it is the ratio that determines the transition between small-sphere-leading and large-sphere-leading regimes; $\delta = \sqrt{\nu/\omega}$ is the oscillatory boundary layer thickness and ν is the kinematic viscosity of the fluid. We carried out simulations in 2D and 3D and found qualitative agreement. We focused on 2D because it allowed us to study a much broader parameter space. The range studied in Re was $0.001 \leq Re \leq 150$. All other parameter ranges (amplitude, radii,*etc.*) are shown in the SM, table S1 [55].

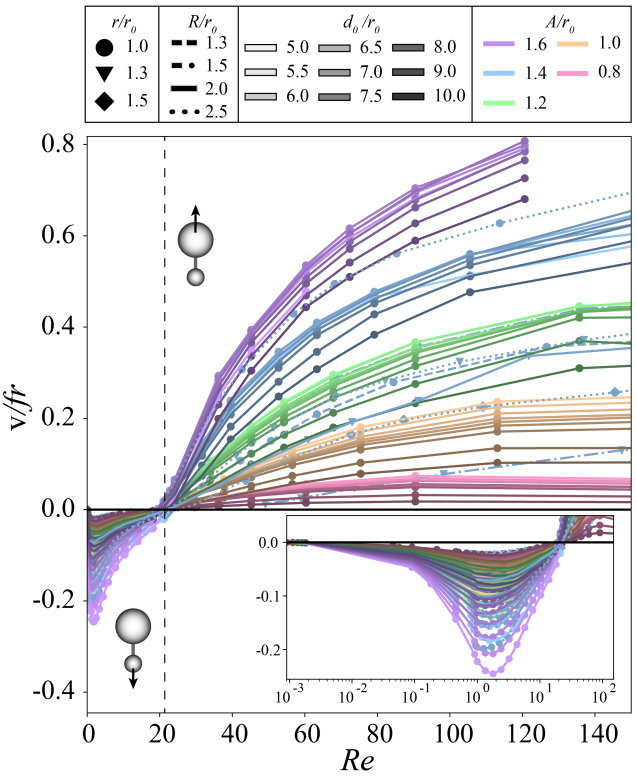

FIG. 2. Velocity of the spherobot as a function of Re in 2D for a range of A, d_0, R, r shown in the legend. The inset shows the small-sphere-leading regime plotted on a semi-log-x scale. Parameters A, d_0, R, and r are non-dimensionalized by the length scale, $r_0 = 0.15$m, the radius for the small sphere. Line color indicates A, line saturation indicates d_0, line style indicates R, and symbols indicate r. Negative velocity indicates swimming in the direction of the small sphere, positive velocity indicates swimming in the direction of the large sphere. Vertical dashed lines denote critical Re for transition.

Results. We initially placed the spherobot in the simulation box at constant A, A_R, A_r, d_0, f, R, r and varied the Re via the kinematic viscosity, ν. As a validation, we ran a simulation at $Re = 0$ and confirmed that the spherobot did not swim because of Purcell's theorem for reciprocal swimmers [48]. As soon as $Re > 0$ (lowest value $Re = 0.001$) the spherobot began to swim in the direction of the small sphere (Fig.2), *i.e.* the small-sphere-leading regime. As Re increased, the speed of the spherobot increased until reaching a maximum at $Re \approx 2$. Above $Re \approx 2$ the spherobot slowed down and eventually had no net displacement (even though the spheres oscillated) at $Re \approx 20$. As Re increased further, the spherobot switched direction to swim with the large sphere on the front, *i.e.* the large-sphere-leading regime, where its in-

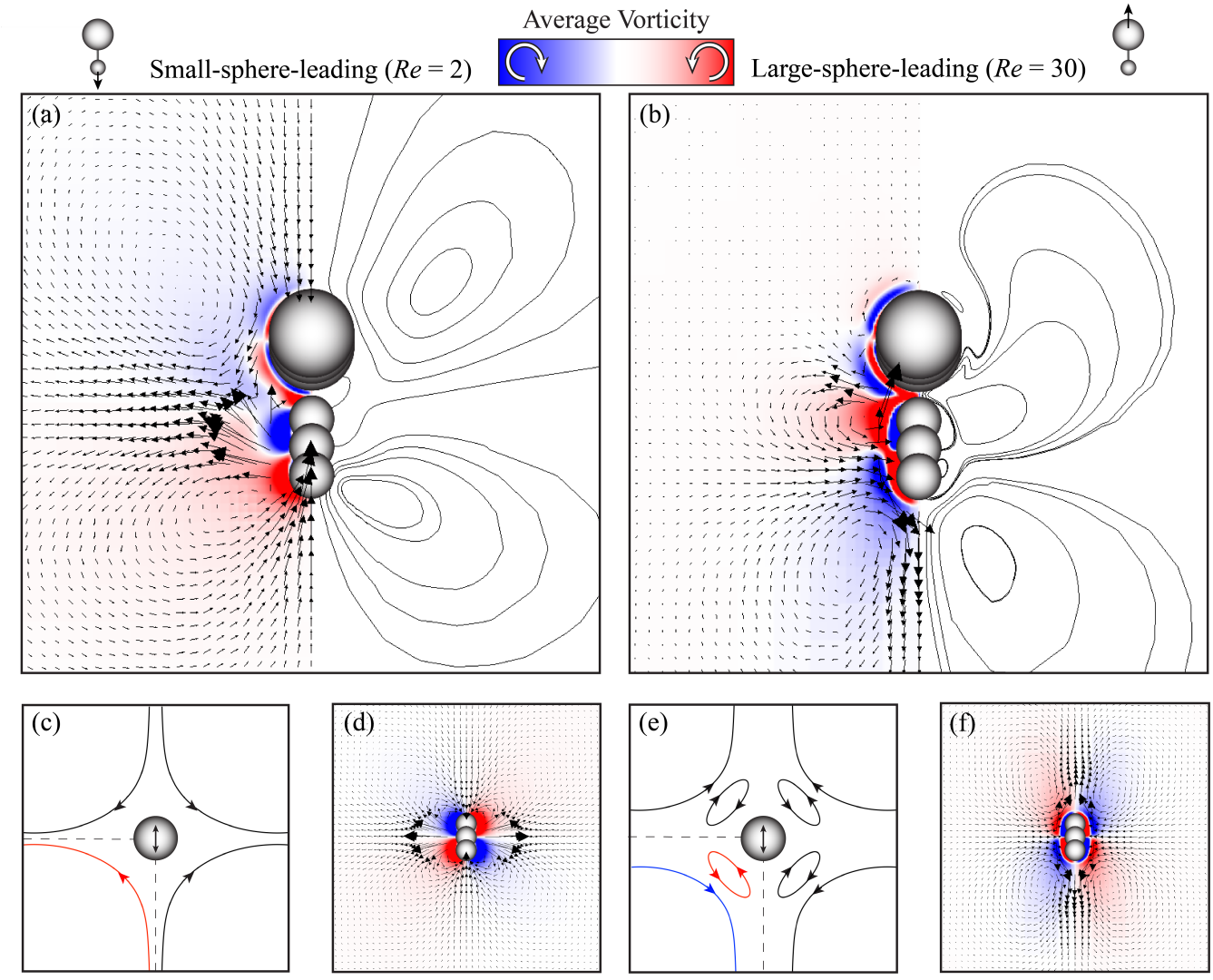

FIG. 3. Left column: Small-sphere-leading regime at $Re = 2$. Right column: Large-sphere-leading regime at $Re = 30$. Spherobot velocity field superimposed with the vorticity field and streamlines in (a) the small-sphere-leading regime and (b) the large-sphere-leading regime. The largest dimensionless velocity magnitude in (a), (b) is $|\mathbf{v_{max}}|/fr = 0.88$. Schematic diagrams showing the reversal of steady streaming flows for one sphere in the limiting cases (c) $\delta \gg r$, and (e) $\delta \ll r$. Due to symmetry the lower left quadrant is indicated with a dashed line. Velocity vector plot superimposed with the vorticity field for one sphere at (d) $Re = 2$ and (f) $Re = 30$. The largest dimensionless velocity magnitude in (d), (f) is $|\mathbf{v_{max}}|/fr = 1.1$. All velocity vectors are scaled the same.

creasing speed started to plateau as Re increased further. We then ran a broader parameter sweep varying R, r, A, A_R, A_r, and d_0 besides the viscosity ν. We found that the transition only depended on the small sphere's radius and amplitude (besides viscosity) and that it was independent of all the other length scales R, A_R and d_0. The transition-point data collapsed (within the scatter on a single, critical dimensionless number $Re = A_r r/\delta^2 \approx 20$ (Fig.2).

To gain insight into the propulsion mechanism and the switch in swimming direction, we turned our attention to the flow fields generated by the spherobot. Based on classical work on steady streaming generated by a single oscillating sphere, we expected each sphere of the spherobot to generate SS flows, which are time-averaged flows by definition. We also anticipated the SS flows around the spherobot to be different than the classical SS flows around a sphere for two reasons. First, the small sphere's oscillation amplitude, A_r, was of the same order of magnitude as the sphere radius, *i.e.* $\epsilon = A_r/r \approx O(1)$ unlike the assumption for classical steady streaming where $\epsilon \ll 1$ [36, 37, 56]. Second, it was unclear what the cumulative SS flows of two spheres oscillating in antiphase should be, as it has only been studied for spheres and cylinders in phase [41, 57–59]. Bearing these considerations in mind, we calculated the time-averaged flow fields

around the spherobot, varying the same parameters as before, (Fig.2). We found that the switch in the swimming direction at $Re \approx 20$ corresponded to the reversal of the SS flows both parallel and perpendicular to the axis of oscillation. Specifically, in the small-sphere-leading regime ($Re < 20$), the fluid, on average, was pulled in towards the spheres along the axis of oscillation and was pushed out away from the spheres along the axis perpendicular to the oscillation, (Fig. 3 (a)). On the contrary, in the large-sphere-leading regime ($Re > 20$), the fluid, on average, did the opposite – it was pushed away from the spheres along the direction of swimming (with a strong downward jet below the small sphere) and was pulled in towards the gap between the spheres in the direction perpendicular-to-swimming (Fig. 3 (b)).

Furthermore, in both regimes it is clear that the velocity vectors along the oscillation axis are larger around the small sphere than the large sphere, (Fig.3). In fact, through control volume analysis we found that for both regimes, the momentum flux on the side of the small sphere was larger than the momentum flux on the side of the large sphere, (the ones along the perpendicular axis generated fluxes that canceled each other). Though initially unexpected, this finding makes sense together with the collapse, which depends on the Re of the small sphere only, (Fig.2). The net momentum flux of course switches direction as the swimming direction switches, (see Fig.S4 [55]). Our data, thus, strongly suggest that the transition in the spherobot's swimming direction is due to the reversal of SS flows, which is associated with the switch in the direction of the net momentum flux [55].

Discussion. To better understand the reversal of SS flows, we will consider what is known for one sphere. Analytic solutions have been obtained under the small-amplitude assumption $A_r \ll r$ and in the two limiting cases relating the sphere radius to the boundary layer thickness, $\delta \gg r$ and $\delta \ll r$. The two limiting cases demonstrate a reversal in direction, shown schematically in Fig.3(c),(e) [36, 37, 56]. In the first case, the boundary layer thickness is much larger than the radius, $\delta \gg r$, (Fig.3(c)). Due to symmetry we describe one quadrant of flow. A single vortex that is the boundary layer is generated near the surface of the sphere, which pulls fluid along the axis of oscillation and pushes fluid out in the perpendicular. In the second case, the boundary layer thickness is much smaller than the radius of the sphere, $\delta \ll r$, (Fig.3(e)). Two vortices are generated swirling in opposite directions. The boundary layer is confined into an inner vortex close to the surface of the sphere (same direction as in the first case) but there is an additional outer vortex in the opposite direction – it pushes fluid out along the axis of oscillation and pulls it in along the perpendicular. The analytical limiting solutions, that we just described, provide us a with qualitative picture; we cannot use them for direct comparison because neither $A_r \ll r$ nor $\delta \gg r$ or $\delta \ll r$ holds true for our system. Instead, we compare our results to experiments and simulations, where $\epsilon = A_r/r = O(1)$ and $r/\delta = O(1)$, as for the spherobot.

Unlike the spherobot where the reversal of flows corresponds to a switch in the direction of swimming, the point where reversal of flows occurs for a single sphere is not well-defined [36, 38, 60, 61]. Experimental observations have reported that they could observe the inner vortex when $r/\delta \leq 4$ [62], while experiments and simulations reported the coexistence of inner and outer vortices with opposing flows for $r/\delta \geq 7$ [62–66]. It was also shown that the reversal of flows depends on the sphere's amplitude, yet a specific scaling was not found [38, 60–62]. Relating all this back to the spherobot, our data collapse gave $Re = A_r r/\delta^2$ as the critical parameter for the transition in swimming direction, a scaling that includes an amplitude dependence, as suggested by previous works. Moreover, we found that when plotting the dimensionless velocity of the spherobot as a function of r/δ, the transition in swimming ($Re \approx 20$) occurred in the range $r/\delta \approx [3.5, 7]$, (see Fig.S7 [55]), again in agreement with previous reports on the reversal of SS flows for a sphere.

We can make an analogy that the large sphere of the spherobot acts like the body of the swimmer while the small sphere acts like the flagellum. In fact, it is really interesting that the SS flows, which are unrelated to the squirmer models, in the small-sphere leading regime resemble the flow field of Stokesian pullers and in the large-sphere leading regime resemble the flow field of Stokesian pushers [67–69]. However, the organisms that swim like pullers and pushers such as algae and bacteria, respectively, have different appendages in order to perform the "pulling" or the "pushing". What is remarkable here is that the geometry of the spherobot does not have to change – the small sphere can act as an effective flagellum that can both "pull" and "push" depending only on the critical parameter $Re = A_r r/\delta^2$. *E.g.* our swimmer can change its amplitude and it will switch swimming direction.

To conclude, we have proposed a model spherobot swimmer that utilizes SS in a novel way, to propel itself. The main findings of the current letter are (i) a transition in the swimming direction that collapses onto a single critical Reynolds number and (ii) the physical mechanism for the transition in swimming is the reversal of SS flows. Based on our findings, we propose that SS can be an important physical mechanism present more generally in motility at Re_{int} both in biological organisms but also when designing artificial swimmers [45, 47, 70, 71]. Finally, we expect to find interesting emergent collective behavior of multiple spherobot swimmers as nonlinearities add up leading to different steady states and patterns.

ACKNOWLEDGMENTS

Acknowledgments. S.K.J. and T.D. contributed equally to this work. D.K. acknowledges the National Science Foundation, grant award DMR-1753148 and

start-up funds by the Department of Applied Physical Sciences at the University of North Carolina at Chapel Hill.

[1] Werner Nachtigall, "Some aspects of Reynolds number effects in animals," Mathematical Methods in the Applied Sciences **24**, 1401–1408 (2001).

[2] Steven Vogel, Life's devices (Princeton University Press, 1988).

[3] Steven Vogel, Life in moving fluids : the physical biology of flow (Princeton University Press, 1994) p. 467.

[4] Wei Wang, Wentao Duan, Suzanne Ahmed, Ayusman Sen, and Thomas E Mallouk, "From one to many: Dynamic assembly and collective behavior of self-propelled colloidal motors," Accounts of chemical research **48**, 1938–1946 (2015).

[5] Debabrata Patra, Samudra Sengupta, Wentao Duan, Hua Zhang, Ryan Pavlick, and Ayusman Sen, "Intelligent, self-powered, drug delivery systems," Nanoscale **5**, 1273–1283 (2013).

[6] Sherif Tolba, Reda Ammar, and Sanguthevar Rajasekaran, "Taking swarms to the field: A framework for underwater mission planning," in Computers and Communication (ISCC) (IEEE, 2015) pp. 1007–1013.

[7] Ryo Fujiwara, Takeshi Kano, and Akio Ishiguro, "Self-swarming robots that exploit hydrodynamical interaction," Advanced Robotics **28**, 639–645 (2014).

[8] Miguel Duarte, Vasco Costa, Jorge Gomes, Tiago Rodrigues, Fernando Silva, Sancho Moura Oliveira, and Anders Lyhne Christensen, "Evolution of collective behaviors for a real swarm of aquatic surface robots," PloS one **11**, e0151834 (2016).

[9] Stephen Childress, Mechanics of swimming and flying (Cambridge University Press, 1981).

[10] Eric Lauga and Thomas R Powers, "The hydrodynamics of swimming microorganisms," Reports on Progress in Physics **72**, 096601 (2009).

[11] Ian K Bartol, Paul S Krueger, William J Stewart, and Joseph T Thompson, "Pulsed jet dynamics of squid hatchlings at intermediate Reynolds numbers." The Journal of Experimental Biology (2009), 10.1242/jeb.033241.

[12] Gregory Herschlag and Laura Miller, "Reynolds number limits for jet propulsion: a numerical study of simplified jellyfish," Journal of theoretical biology **285**, 84–95 (2011).

[13] Stefan Kern and Petros Koumoutsakos, "Simulations of optimized anguilliform swimming," Journal of Experimental Biology **209**, 4841–4857 (2006).

[14] Lee A Fuiman and Paul W Webb, "Ontogeny of routine swimming activity and performance in zebra danios (Teleostei: Cyprinidae)," Animal Behaviour **36**, 250–261 (1988).

[15] J. Sznitman, X. Shen, R. Sznitman, and P. E. Arratia, "Propulsive force measurements and flow behavior of undulatory swimmers at low Reynolds number," Physics of Fluids **22**, 121901 (2010).

[16] Matthew J McHenry, Emanuel Azizi, and James A Strother, "The hydrodynamics of locomotion at intermediate Reynolds numbers: undulatory swimming in ascidian larvae (Botrylloides sp.)," Journal of Experimental Biology **206**, 327–343 (2003).

[17] Amneet Pal Singh Bhalla, Boyce E Griffith, and Neelesh A Patankar, "A forced damped oscillation framework for undulatory swimming provides new insights into how propulsion arises in active and passive swimming," PLoS computational biology **9**, e1003097 (2013).

[18] J Rudi Strickler, "Swimming of planktonic Cyclops species (Copepoda, Crustacea): pattern, movements and their control," in Swimming and flying in nature (Springer, 1975) pp. 599–613.

[19] R W Blake, "Hydrodynamics of swimming in the water boatman, Cenocorixa bifida," Canadian journal of zoology **64**, 1606–1613 (1986).

[20] Brendan J Borrell, Jeremy A Goldbogen, and Robert Dudley, "Aquatic wing flapping at low Reynolds numbers: swimming kinematics of the Antarctic pteropod, Clione antarctica," Journal of Experimental Biology **208**, 2939–2949 (2005).

[21] Brad J Gemmell, Houshuo Jiang, and Edward J Buskey, "A tale of the ciliate tail: Investigation into the adaptive significance of this sub-cellular structure," in Proc. R. Soc. B, Vol. 282 (The Royal Society, 2015) p. 20150770.

[22] Houshuo Jiang, "Why does the jumping ciliate Mesodinium rubrum possess an equatorially located propulsive ciliary belt?" Journal of plankton research , fbr007 (2011).

[23] Eric Kunze, John F Dower, Ian Beveridge, Richard Dewey, and Kevin P Bartlett, "Observations of biologically generated turbulence in a coastal inlet," Science **313**, 1768–1770 (2006).

[24] Monica M Wilhelmus and John O Dabiri, "Observations of large-scale fluid transport by laser-guided plankton aggregations a)," Physics of Fluids **26**, 101302 (2014).

[25] Janna C Nawroth and John O Dabiri, "Induced drift by a self-propelled swimmer at intermediate Reynolds numbers," Physics of Fluids **26**, Art–No (2014).

[26] Isabel A Houghton, Jeffrey R Koseff, Stephen G Monismith, and John O Dabiri, "Vertically migrating swimmers generate aggregation-scale eddies in a stratified column," Nature , 1 (2018).

[27] Nicholas G Chisholm and Aditya S Khair, "Partial drift volume due to a self-propelled swimmer," Physical Review Fluids **3**, 014501 (2018).

[28] Shannon K Jones, Young JJ Yun, Tyson L Hedrick, Boyce E Griffith, and Laura A Miller, "Bristles reduce the force required to fling wings apart in the smallest insects," Journal of Experimental Biology **219**, 3759–3772 (2016).

[29] Eric Lauga, "Continuous breakdown of purcell's scallop theorem with inertia," Physics of Fluids **19**, 061703 (2007).

[30] S Wang and A Ardekani, "Inertial squirmer," Physics of Fluids **24**, 101902 (2012).

[31] Aditya S Khair and Nicholas G Chisholm, "Expansions at small reynolds numbers for the locomotion of a spherical squirmer," Physics of Fluids **26**, 011902 (2014).

[32] Nicholas G. Chisholm, Dominique Legendre, Eric Lauga, and Aditya S. Khair, "A squirmer across reynolds numbers," Journal of Fluid Mechanics **796**, 233–256 (2016).

[33] Gaojin Li, Anca Ostace, and Arezoo M. Ardekani, "Hydrodynamic interaction of swimming organisms in an inertial regime," Physical Review E **94**, 053104 (2016).

[34] Jie Zhang, Nan-Sheng Liu, and Xi-Yun Lu, "Locomotion of a passively flapping flat plate," Journal of Fluid Mechanics **659**, 43–68 (2010).

[35] Saverio E Spagnolie, Lionel Moret, Michael J Shelley, and Jun Zhang, "Surprising behaviors in flapping locomotion with passive pitching," Physics of Fluids **22**, 041903 (2010).

[36] N. Riley, "On a sphere oscillating in a viscous fluid," Quart. Journ. Mech. and Applied Math **XIX**, 461–472 (1966).

[37] N Riley, "Steady streaming," Annual Review of Fluid Mechanics **33**, 43–65 (2001).

[38] Eugene J Chang and Martin R Maxey, "Unsteady flow about a sphere at low to moderate reynolds number. part 1. oscillatory motion," Journal of Fluid Mechanics **277**, 347–379 (1994).

[39] Charlotte W Kotas, Minami Yoda, and Peter H Rogers, "Visualization of steady streaming near oscillating spheroids," Experiments in fluids **42**, 111–121 (2007).

[40] Florian Otto, Emmalee K Riegler, and Greg A Voth, "Measurements of the steady streaming flow around oscillating spheres using three dimensional particle tracking velocimetry," Physics of fluids **20**, 093304 (2008).

[41] D. Klotsa, Michael R. Swift, R. M. Bowley, and P. J. King, "Interaction of spheres in oscillatory fluid flows," Phys. Rev. E **76**, 056314 (2007).

[42] H. S. Wright, Michael R. Swift, and P. J. King, "Migration of an asymmetric dimer in oscillatory fluid flow," Phys. Rev. E **78**, 036311 (2008).

[43] D. Klotsa, Michael R. Swift, R. M. Bowley, and P. J. King, "Chain formation of spheres in oscillatory fluid flows," Phys. Rev. E **79**, 021302 (2009).

[44] Daphne Klotsa, Kyle A Baldwin, Richard JA Hill, Roger M Bowley, and Michael R Swift, "Propulsion of a two-sphere swimmer," Physical review letters **115**, 248102 (2015).

[45] Tamsin A. Spelman and Eric Lauga, "Arbitrary axisymmetric steady streaming: flow, force and propulsion," Journal of Engineering Mathematics **105**, 31–65 (2017).

[46] Barry R Lutz, Jian Chen, and Daniel T Schwartz, "Hydrodynamic tweezers: 1. noncontact trapping of single cells using steady streaming microeddies," Analytical chemistry **78**, 5429–5435 (2006).

[47] Kurt M. Ehlers and Jair Koiller, "Could cell membranes produce acoustic streaming? making the case for synechococcus self-propulsion," Mathematical and Computer Modelling **53**, 1489 – 1504 (2011), mathematical Methods and Modelling of Biophysical Phenomena.

[48] E. M. Purcell, "Life at low Reynolds number," American Journal of Physics **45**, 3–11 (1977).

[49] B. Kallemov, A. P. S. Bhalla, B. E. Griffith, and A. Donev, "An immersed boundary method for rigid bodies," Comm Appl Math Comput Sci **11**, 79–141 (2016).

[50] F. Balboa Usabiaga, B. Kallemov, B. Delmotte, A. P. S. Bhalla, B. E. Griffith, and A. Donev, "Hydrodynamics of suspensions of passive and active rigid particles: a rigid multiblob approach," Communications in Applied Mathematics and Computational Science **11**, 217–296 (2016).

[51] Boyce E Griffith, Richard D Hornung, David M McQueen, and Charles S Peskin, "An adaptive, formally second order accurate version of the immersed boundary method," Journal of Computational Physics **223**, 10–49 (2007).

[52] "IBAMR: An adaptive and distributed-memory parallel implementation of the immersed boundary method," `https://github.com/IBAMR/IBAMR`.

[53] Charles S. Peskin, "The immersed boundary method," Acta Numerica **11**, 479–517 (2002).

[54] Hank Childs, Eric Brugger, Brad Whitlock, Jeremy Meredith, Sean Ahern, David Pugmire, Kathleen Biagas, Mark Miller, Cyrus Harrison, Gunther H. Weber, Hari Krishnan, Thomas Fogal, Allen Sanderson, Christoph Garth, E. Wes Bethel, David Camp, Oliver Rübel, Marc Durant, Jean M. Favre, and Paul Navrátil, "VisIt: An End-User Tool For Visualizing and Analyzing Very Large Data," in High Performance Visualization-Enabling Extreme-Scale Scientific In (2012) pp. 357–372.

[55] See Supplementary Material for more details on methods, additional figures and movies of the spherobot.

[56] J Milton Andres and Uno Ingard, "Acoustic streaming at low reynolds numbers," The Journal of the Acoustical Society of America **25**, 932–938 (1953).

[57] Z Zapryanov, Zh Kozhoukharova, and A Iordanova, "On the hydrodynamic interaction of two circular cylinders oscillating in a viscous fluid," Zeitschrift für angewandte Mathematik und Physik ZAMP **39**, 204–220 (1988).

[58] SS Tabakova and ZD Zapryanov, "On the hydrodynamic interaction of two spheres oscillating in a viscous fluid. i. axisymmetrical case," Zeitschrift für angewandte Mathematik und Physik ZAMP **33**, 344–357 (1982).

[59] SS Tabakova and ZD Zapryanov, "On the hydrodynamic interaction of two spheres oscillating in a viscous fluid. ii. three dimensional case," Zeitschrift für Angewandte Mathematik und Physik (ZAMP) **33**, 487–502 (1982).

[60] R.S. Alassar and H.M. Badr, "Oscillating viscous flow over a sphere," Computers & Fluids **26**, 661–682 (1997).

[61] H. M. Blackburn, "Mass and momentum transport from a sphere in steady and oscillatory flows," Physics of Fluids **14**, 3997–4011 (2002), https://doi.org/10.1063/1.1510448.

[62] Masakazu Tatsuno, "Circulatory streaming around an oscillating circular cylinder at low reynolds numbers," Journal of the Physical Society of Japan **35**, 915–920 (1973).

[63] W Coenen and N Riley, "Oscillatory flow about a cylinder pair," Quarterly journal of mechanics and applied mathematics **62**, 53–66 (2008).

[64] Masakazu Tatsuno, "Secondary flow induced by a circular cylinder performing unharmonic oscillations," Journal of the Physical Society of Japan **50**, 330–337 (1981).

[65] Tore Olsen, "Rotational flow of a viscous fluid," The Journal of the Acoustical Society of America **28**, 313–314 (1956).

[66] J Holtsmark, I Johnsen, To Sikkeland, and S Skavlem, "Boundary layer flow near a cylindrical obstacle in an oscillating, incompressible fluid," The journal of the acoustical society of America **26**, 26–39 (1954).

[67] MJ Lighthill, "On the squirming motion of nearly spherical deformable bodies through liquids at very small reynolds numbers," Communications on Pure and Applied Mathematics **5**, 109–118 (1952).

[68] J. R. Blake, "A spherical envelope approach to ciliary propulsion," Journal of Fluid Mechanics **46**, 199208 (1971).

[69] T. J. Pedley, "Spherical squirmers: models for swimming micro-organisms," IMA Journal of Applied Mathematics **81**, 488–521 (2016).

[70] Kurt Ehlers and Jair Koiller, "Synechococcus as a "singing" bacterium: biology inspired by micro-engineered acoustic streaming devices," (2009), arXiv:0903.3781.

[71] François Nadal and Eric Lauga, "Asymmetric steady streaming as a mechanism for acoustic propulsion of rigid bodies," Physics of Fluids **26**, 082001 (2014).